Nanoscale

Accepted Manuscript

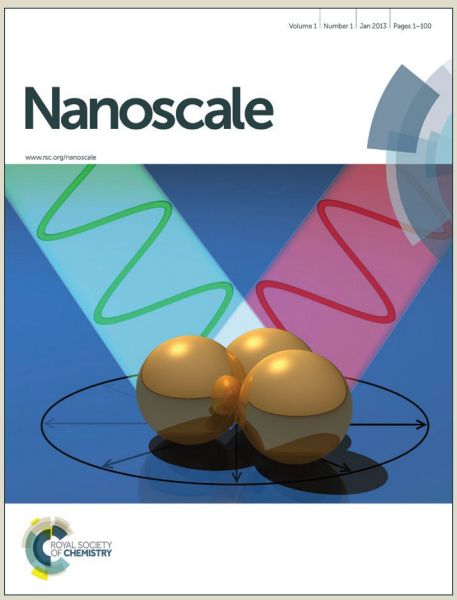

ROYAL SOCIETY OF CHEMISTRY

www.rsc.org/nanoscale

Journal Name

ARTICLE

Reversible switching of structural and plasmonic properties of liquid-crystalline gold nanoparticle assemblies

Received 00th January 20xx,
Accepted 00th January 20xx

DOI: 10.1039/x0xx00000x

www.rsc.org/

W. Lewandowski,[a]* T. Łojewska,[a] P. Szustakiewicz,[a] J. Mieczkowski,[a] D. Pociecha[a]

Hybrid materials built of spherical gold nanoparticles with three different sizes and covered with (pro)mesogenic molecules have been prepared. Small-angle X-ray diffraction studies showed that after thermal annealing most of the obtained materials formed long-range ordered assemblies. Variation of the (pro)mesogenic ligands architecture enabled to achieve a switchable material, which could be reversibly reconfigured between 3D long-range ordered structures with tetragonal and face centred cubic symmetries. This structural reconfiguration induces changes to the plasmonic response of the material. The work demonstrates that it is possible to use LC-based self-assembling phenomena to prepare dynamic materials with structural properties important for the development of active plasmonic metamaterials.

Introduction

Active plasmonic materials built of metal nanoparticles (NPs) attract considerable interest[1] due to emerging applications in broadband metamaterials,[2] nanoelectronics,[3,4] waveguiding[5] and photonics[6,7,8,9]. These technologies capitalize on surface plasmon resonance of individual metal NPs and inter-particle coupling. However, full exploitation of the applicative potential requires fabrication methods yielding structures with high metal filling factors, precisely controlled interparticle spacing, reversible switching and short response times.[10,11,12,13]
Various methods were developed to achieve active plasmonic materials made of NPs, e.g. embedding NPs in a stimuli responsive[14–16] or stretchable[17] polymer matrix, using reversible aggregation-dispersion process,[18–20] gel-sol transition,[21] the Langmuir–Blodgett technique,[22] as well as magnetically[23,24] and electrically[25] addressable mesophases. Mesophases can be also addressed indirectly using photothermal effect of organo-soluble plasmonic gold nanorods.[26,27] These methods provide important paths towards functional materials, however they often rely on dilute NPs systems, NP spacing is controlled only on short-range or switching is non-reversible. Thus, further progress towards active, plasmonic nanoscale architectures is required.
Recently, a feasible approach to tackle the problems of dynamic nanoparticle materials has been proposed – the use of shape-shifting NPs.[28–31] Realization of this concept is possible by using thermotropic liquid crystals (LCs) as nanoparticle surface ligands - in this case reversible reconfiguration of nanoparticle-based material derives from switchable shape of the organic coating of nanoparticles. Thus, spatial distribution of particles is changed without affecting the shape of the metallic nanocluster. The LC-based strategy has already proven to be a versatile self-assembly approach towards functional materials[32–41] e.g. with anisotropic plasmonic properties.[42,43] Importantly, this approach enabled preparation of switchable materials with magneto-,[44] photo-[45,46] and temperature-responsiveness[47], recently dynamically reconfigurable epsilon-near-zero metamaterial was also reported.[48] Unfortunately, the up-to-date reported active plasmonic materials based on LC-approach included either short-range ordered phases or required long switching times.[34,48,49] Thus, obtaining reconfigurability between long range ordered structures and improving the switching kinetics are two important challenges that have to be faced by LC-NPs technology.[50] These properties are especially important in the context of metamaterial research since internal order is one of the key parameters for achieving metamaterial behavior while future of metamaterials lies in reconfigurable systems.[2,51]
In this article, we aimed to overcome the above mentioned limitations by designing a series of hybrid nanoparticles with metallic core and (pro)mesogenic surface ligands. By exploring ligands' architecture we were able to prepare a thermally tunable, plasmonic material with relatively fast response to thermal stimuli, at least one order of magnitude faster than the current state of the art. Moreover, this material exhibits switchability between two long-range ordered structures as probed by x-ray diffraction. Consequently, the novel hybrid materials exhibit reversible shifts of plasmonic resonances as followed by in-situ spectroscopic measurements.

Experimental section

Materials and methods for organic synthesis

[a] 1 Pasteura st., Faculty of Chemistry, University of Warsaw, 02-093 Warsaw, Poland
Electronic Supplementary Information (ESI) available: [details of any supplementary information available should be included here]. See DOI: 10.1039/x0xx00000x

Solvents and substrates were obtained from Sigma-Aldrich. Before use solvents were dried over activated molecular sieves for 24h. Substrates were used without further purification. All reactions were carried out under nitrogen (N_2) atmosphere in dried glassware and assuring efficient magnetic stirring. Purification of reaction products was carried out by column chromatography using RushanTaiyang silica gel 60 (230-400 mesh) at atmospheric pressure or by crystallization if possible. Analytical thin-layer chromatography (TLC) was performed using Silica Gel 60 Å F254 (Merck) pre-coated glass plater (0.25 mm thickness) and visualized using iodine vapor and/or UV lamp (254 nm). Yields refer to chromatographically and spectroscopically (1H NMR) homogeneous materials.

The ^{1}H NMR and ^{13}C NMR spectra were recorded at either 200 MHz or 500 MHz NMR Varian Unity Plus. Proton chemical shifts are reported in ppm (δ) relative to the internal standard - tetramethylsilane (TMS δ =0.00 ppm). Carbon chemical shifts are reported in ppm (δ) relative to the residual solvent signal (CDCl3, δ =77.0 ppm). Detailed synthetic procedures and analyses are given in the SI.

Nanoparticle synthesis

Silver (**S5**) and gold (**G4**) nanoclusters with dodecanethiol coating were prepared using a modified literature method.[52] Shortly, dodecylamine (1.5 g) solution in cyclohexane (50 ml) was stirred for 10 min with 12 ml aqueous formaldehyde (37%). The organic phase was separated out and washed twice with water (2x50 ml). Then, aqueous solution of $AgNO_3$ (0.4 g $AgNO_3$ in 20 ml H_2O) or $HAuCl_4$ (80 mg in 20 ml H_2O) was added, left to stir for 40 min after which dodecanethiol (0.3 molar eq. of dodecylamine) was added and the reaction was stirred overnight. Organic phase was separated and NPs were precipitated by addition of 100 ml of ethanol. The precipitate was centrifuged, collected, dissolved in a small amount of cyclohexane (10 ml) and again the precipitation procedure was repeated.

Small gold nanoparticles (**G2**) were obtained using a modified literature method.[53] An aqueous solution of $HAuCl_4$ (50 mL, 145 mM) was mixed with a solution of methyltrioctylammonium bromide in toluene (50 mL, 125 mM). The two-phase mixture was vigorously stirred. Consequently, phases were separated and decanethiol (1.4 g, 8.0 mmol) was then added to the organic phase and stirred for 20 min. Then, freshly prepared aqueous solution of sodium borohydride (50 mL, 0.4 M) was quickly added. After further stirring for 3 h the organic phase was separated, washed with water (2 x 100 mL), and precipitated with 200 mL of ethanol. The precipitate was washed twice with ethanol (100 mL) and dissolved in cyclohexane.

Ligand exchange reaction on nanoparticles

Dodecanethiol coated NPs were used as the starting material for the preparation of hybrid NPs. To 20mg of NPs dissolved in 15 ml hexane/DCM mixture (1/1, v/v) 20 mg of given promesogenic ligand (L1-3) was added. The reaction proceeded at room temperature for 12 h. Then, NPs were precipitated with 20 ml of acetone and centrifuged. Supernatant containing unbound thiol ligands was discarded. The precipitate was dissolved in 1ml of warm hexane and centrifuged after cooling down; then, the process was repeated. This washing procedure was repeated until no traces of free mesogenic ligand remained, as determined by thin-layer chromatography. The obtained nanoparticles are denoted as LX_Y, where LX stands for L1-3, while Y refers to the type of nanoparticle core (G2, G4, S5).

SAXRD measurements

The small angle X-ray diffraction (SAXRD) and scattering (SAXS) experiments were performed with the Bruker Nanostar system (CuKα radiation, parallel beam formed by cross-coupled Goebel mirrors and 3-pinhole collimation system, area detector VANTEC 2000). The temperature of the sample was controlled with precision of 0.1 K. Samples were prepared in thin-walled glass capillaries or as a thin films on kapton tape substrate. For all samples temperature dependent measurements were performed in the same manner – data was collected every 5 K for 300 s with 40 K/min heating rate between consecutive data collection points. Quasi-monodomain samples were prepared by mechanical shearing at elevated temperatures (below the phase transition point).

Transmission electron micrography

Transmission electron micrography was performed using Zeiss Libra 120 microscope, with LaB6 cathode, equipped with OMEGA internal columnar filters and CCD camera. For TEM imaging materials were dropcasted onto TEM grids and thermally annealed.

UV-Vis spectroscopy

The UV-Vis spectrum was measured using a Cary 5000 spectrometer (Agilent). The solutions of functionalized particles in dichloromethane were held in standard PMMA cuvettes (VWR) with a 10 mm optical path, while the aggregates were recorded on a quartz substrate in a transmission mode.

Thermogravimetric analysis of nanoparticles

Thermogravimetric (TGA) analysis were performed with a TA Q50 V20.13 (TA Instruments) analyzer. The measurements were carried out in 20-600 °C range with 10 K/min heating rate in air.

The weight loss for alkyl-coated gold nanoparticles (below 250 °C) was attributed to the removal of the organic shell and recalculated to the number of surface alkyl thiols as outlined below. TGA traces for hybrid nanoparticles revealed substantially larger weight losses in two distinct steps. The first one, below 250 °C can be attributed to the removal of alkyl thiol molecules. A wider peak at higher temperature values (>250 °C) is due to the removal of L molecules.

To convert the mass loss measured by the TGA measurements to surface ligand stoichiometry we first calculated the mass of single metal spheres for different types of nanoparticles, using the diameter derived from SAXS and TEM and the bulk density of metals. The mass of organic matter (M_{org}) removed from a

single nanoparticle was calculated using % of mass left after the analysis (%M_{left}) and % of mass loss (%M_{loss}): $M_{org} = M_{Ag(or\ Au)}$ /%M_{left}*%M_{loss}. To determine the number of ligands per nanoparticle M_{org} has to be divided by the mass (in [g]) of the ligand responsible for the given mass drop. For nanoparticles after the ligand exchange reactions mass losses below and above 250°C were treated separately. If it was not possible to discriminate the two signals the total number of ligands was assumed to be the same as in the case of alkyl-coated nanoparticles, and then the total mass drop was recalculated to the numbers of alkyl and promesogenic ligands.

Results and discussion

Hybrid nanoparticle design and synthesis

Properties of LC-nanoparticle assemblies depend strongly on the structure of surface ligands as well as nanoparticle size and shape. Here, we undertake a new approach to influence the assembly of nanoparticles; namely, we vary the overall geometry and flexibility of ligands by changing one of the aromatic cores of the molecules. Such changes in connectivity were shown to be important factor determining type of organic liquid-crystalline phases, however they are yet unexplored in LC-nanoparticle hybrid systems. It should be noted, that up-to-date both rod-like and bent-core LC ligands were used for grafting NPs, however difference in their structures makes direct comparisons difficult.[36,37,39]

In our work we have designed three novel, potentially mesogenic, surface ligands (**L1**, **L2**, **L3, Fig. 1.**) and investigated their ability to induce formation of tunable assemblies of hybrid NPs. Details of the organic synthesis are given in the SI. A three-aromatic ring core of the ligands was chosen since switching between different ordered structures (polymorphism of mesophases) was already observed for similar LC compounds.[54] Furthermore, terminal 16-carbon-long alkyl chains assured fluidity and relative flexibility of the ligands which is necessary for switching the shape of the organic coating. Only one of the obtained molecules – **L2**, exhibited liquid-crystalline properties with the phase sequence: Iso 148°C N 138°C SmC. The other two molecules melt directly to isotropic liquid. Although **L1** and **L3** did not show LC phases, they can be called promesogenic as both supported formation of long-range ordered nanoparticle assemblies.

For the preparation of hybrid materials we have used three types of nanoparticles: 2.2 and 4.4 nm diameter Au NPs (**G2** and **G4**, respectively) as well as 4.8 nm diameter Ag NPs (**S5**). This allowed us to probe versatility of the ligands in inducing formation of switchable assemblies, which is important due to size- and shape-dependent properties of nanoparticles.[55,56] It should be noted that **G2** nanoclusters do not exhibit plasmonic properties, however they were widely used for preparation of LC-hybrid nanoparticles since their small size promotes formation of long-range-ordered phases. Thus, we used **G2**-based hybrid nanoparticles as control samples enabling us to identify ligands that support formation of switchable assemblies.

Synthetic methods for NPs' preparation were chosen so as to prepare nanoclusters soluble in organic solvents, covered with dodecanethiol and with size disparity below 10%. **G2** were synthesized using slightly modified Brust-Schiffrin method,[53] **G4** and **S5** were obtained by modified Wang strategy.[52]

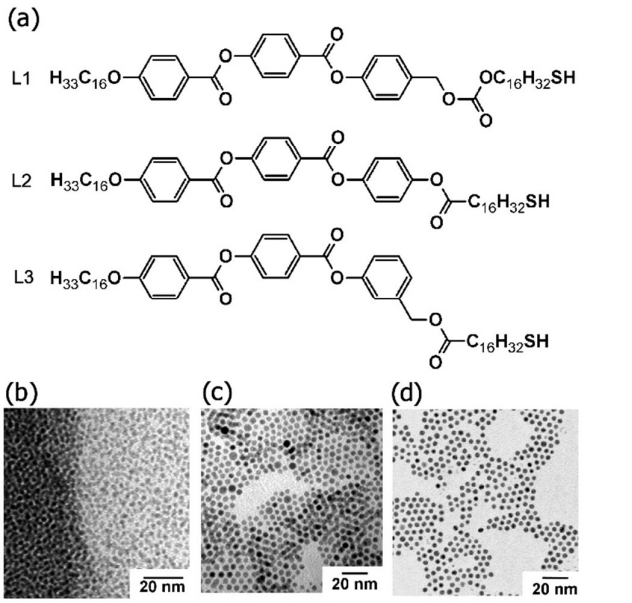

Figure 1. Molecular structures of (pro)mesogenic ligands **L1**, **L2** and **L3** used for grafting nanoparticles and TEM images of metal nanoparticles:(b) **G2**, (c) **G4** and (d) **S5** used to prepare hybrid materials.

In the next step, the synthesized particles were partially covered with organic molecules **L1**-**L3** in a ligand exchange process. Conditions of the reaction were kept so as to assure ca. 35-45% exchange of dodecanethiol molecules to promesogenic species, yielding hybrid nanoparticles. The exchange rate was verified using thermogravimetric measurements (TGA) as previously described[48] (see the SI for details).

Using TGA results we have also calculated volume fraction of the metal in hybrid materials. Depending on the nanoparticle diameter the calculated values varied between 6 to 17% for hybrid NPs based on **G2** and **G4/S5** samples, respectively. Importantly, the values are in the range required for obtaining metamaterial properties.

Nanoparticle aggregates based on L1 molecules

First, we investigated the assemblies of hybrid nanoparticles based on **L1** molecules using small angle X-ray measurements (SAXRD). Portions of nanoparticle solutions were dropcasted onto kapton foil and annealed at 130 °C.

For the hybrid material **L1_G2** SAXRD studies of an annealed sample revealed diffractogram characteristic for a lamellar system. The phase assignment was confirmed by experiments performed for the samples aligned by shearing, their XRD

patterns showed set of commensurate Bragg reflections along the direction perpendicular to shearing, corresponding to periodicity d = 7.4 nm, and a diffused signal parallel to the shearing direction, centered at 3.3 nm. The signals correspond to inter- and in-layer particle distance, respectively. Formation of the lamellar structure is driven by the inhomogeneous distribution of thiol molecules at the NPs surface – LC ligands are collected mainly above and below metal spheres , defining the inter-layer periodicity; distance between particles within the layer is determined primarily by the length of the n-alkylthiols.

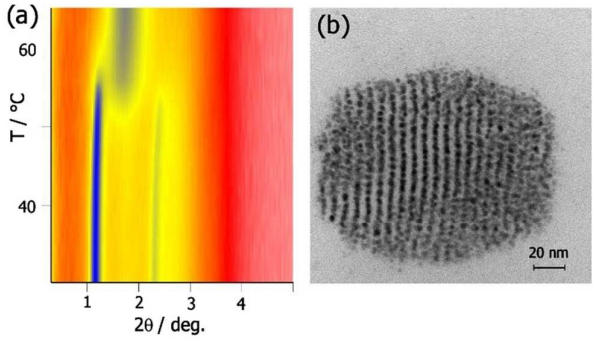

Figure 2. Structural characterization of L1_G2 material. a) Temperature evolution of SAXRD pattern and b) TEM image of an annealed sample.

Further confirmation of lamellar ordering of nanoparticles was obtained using transmission electron microscopy. Small portion of **L1_G2** nanoparticle solution was dropcasted onto TEM grid and thermally annealed. Images of this sample (Fig. 2b) revealed rows of nanoparticles with ca. 7.5 nm inter-row distance, which corresponds well to inter-layer spacing determined with SAXRD measurements.

In order to evaluate influence of temperature on the particles assemblies we performed temperature-dependent SAXRD measurements (Fig. 2a). Interestingly, at ca. 55 °C phase transition was observed after which only one, relatively broad signal centered at 5.0 nm was observed in the XRD patterns indicating formation of an isotropic phase with only short-range positional order. Notably, this is close the lowest temperatures at which a phase transition for LC-NPs has been observed to-date.[57]

For the material **L1_G4** SAXRD measurements of annealed sample revealed two relatively broad reflections in the ratio close to $1:3^{1/2}$ which can indicate short-range 2D hexagonal structure of nanoparticles. Positions of the peaks were temperature independent (Fig. S3a).

In the case of **L1_S5** material SAXRD measurements of an annealed samples revealed one, relatively wide diffraction signal which indicates that metallic particles are ordered on a short-range only (Fig. S3a). The mean interparticle distance (changing in the range 9.0 – 10.5 nm as determined with temperature-dependent SAXRD) was found considerably larger than for corresponding NPs covered with dodecanethiol molecules exclusively, which is reasonable since **L1** ligands are larger than alkanethiols. As the interparticle distance in **L1_S5** was relatively large its changes with temperature by ca. 15% did not influence plasmonic band position significantly.

The performed measurements for **L1**-based hybrid nanoparticles confirmed that the chosen class of (pro)mesogenic ligands is promising in achieving dynamic control over nanoparticle spacing. However, switchability was only found for **L1_G2** material and it was of long-to-short-range order type. Thus, further work was needed to obtain switching between long-range ordered assemblies of plasmonic nanoparticles.

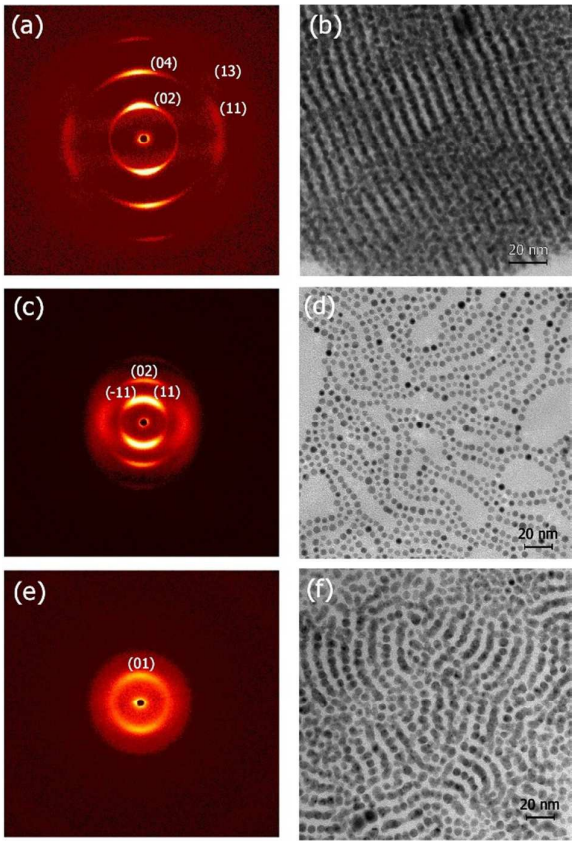

Figure 3. 2D SAXRD patterns taken for aligned samples and corresponding TEM images for **L2**-based hybrid nanoparticles: (a, b) **L2_G2**, (c, d) **L2_G4** and (e, f) **L2_S5**.

Nanoparticle aggregates based on L2 molecules

One can speculate that the possible reasons for the rather unsuccessful use of **L1**-based hybrid materials could be too flexible group attaching the mercapto-functionalized chain to the three-phenyl-rings core of the **L1** molecule. Therefore, we have decided to synthesize organic compound (**L2**) similar to **L1** but devoid of CH_2 moiety in the phenyl ring proximate to nanoparticle surface. The **L2** molecule was then used to prepare hybrid materials using alkanethiol coated nanoparticles (yielding **L2_G2**, **L2_G4** and **L2_S5** materials). For all these materials SAXRD measurements of annealed samples revealed narrow reflections confirming formation of long-range ordered structures. The phase assignment was based on analysis of the patterns registered for monodomain samples aligned by shearing at elevated temperature (ca. 80 °C).

SAXRD measurements of an aligned sample of **L2_G2** material (Fig. 3a) revealed series of 4 commensurate reflections along direction perpendicular to shearing, with basic periodicity 7.35 nm, and two additional signals, at 3.21 nm and 2.74 nm, in direction oblique to shearing. The pattern could be well indexed assuming centered rectangular unit cell (2D) with parameters a = 3.3 nm and c = 14.7 nm. The structure can be interpreted as ABA stacking of NPs' rich layers, with the distance between layers 7.35 nm. Within each layer metallic clusters form most probably hexagonal arrays with mean distance 3.8 nm. To

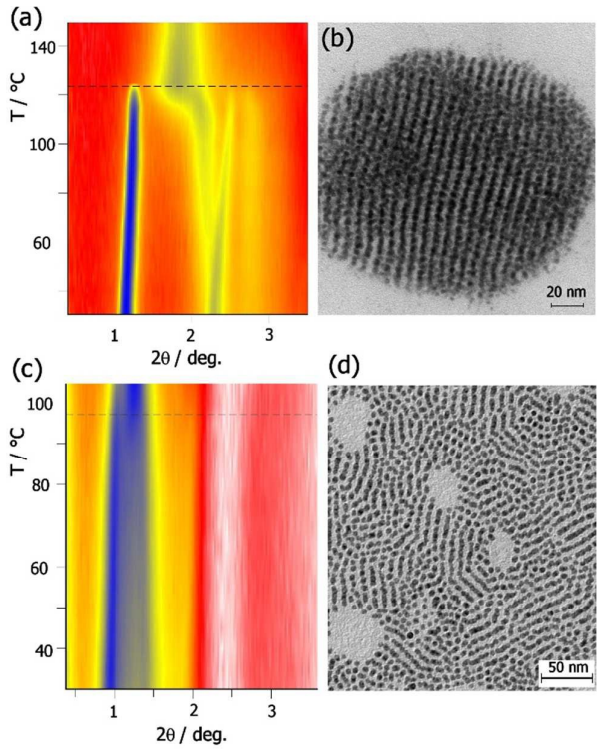

Figure 4. Temperature evolution of SAXRD pattern and corresponding TEM images for annealed **L3**-based hybrid nanoparticles: (a, b) **L3_G2** and (c, d) **L3_S5**.

further confirm the phase assignment TEM was used, micrographs of thermally annealed **L2_G2** sample (Fig. 3b) revealed layers of nanoparticles with 7.5 nm inter-layer spacing which corresponds well to the results from X-ray measurements.

SAXRD pattern of aligned **L2_G4** sample (Fig. 3c) showed a series of incommensurate signals along the direction normal to the shearing direction (the lowest angle signal exhibited weak azimuthal splitting) and a diffused signal along the shearing direction. Such pattern could be ascribed to a modulated lamellar structure with layer spacing 11.6 nm and periodicity of in-plane modulation 24.2 nm. Within the plane neighbouring particle positions are correlated over short-range only, with mean inter-particle distance of 6.4 nm. TEM images (Fig. 3d) did not reveal more details of the assembly, and only evidenced a clear tendency toward lamellar organization of nanoparticles.

For **L2_S5** material XRD experiment performed for partially aligned sample revealed lamellar organization, as evidenced by Bragg reflections in the direction perpendicular to the shearing.

Additional diffused signal centered at 5.5 nm reflected liquid-like organization of nanoparticles within the plane. The phase assignment was further supported by TEM imaging (Fig. 3f) – layers of nanoclusters with ca. 9.1 nm spacing were observed.

Since **L2**-based hybrid materials exhibit internal long-range order, we decided to investigate whether it is possible to switch spatial arrangement of nanoparticles by changing temperature. For this purpose temperature dependent SAXRD measurements were performed. The structure of **L2_G4** material showed almost no changes with temperature, only slight narrowing of the XRD signals was observed due to thermal annealing of the sample (Fig. S3d).

Similarly, for **L2_S5** material no change of structure was observed up to 150 °C when the material started to decompose.

However, for **L2_G2** XRD studies performed on heating (Fig. S3c) evidenced the stability of the structure up to 130 °C, while above this temperature a transition took place, most probably to lamellar (1D) structure. Further heating above 150 °C resulted in sample decomposition. Importantly, the phase transition was of ordered-to-ordered type, as aimed in this study. However, since the small Au particles (**G2**) are not plasmonic the observed switchability is structural, but not functional. Thus, we have decided to redesign the (pro)mesogenic molecule and synthesized ligand **L3**.

Nanoparticle aggregates based on L3 molecules

L3 molecule does not exhibit liquid-crystalline behavior, it melts directly to the isotropic liquid at 78 °C. Lowering of clearing transition temperature in comparison to **L1** and **L2** was achieved by substitution of the chain to the phenyl ring at meta-position instead of para-substitution used in **L1** and **L2** molecules, that modified the overall molecular geometry from rod-like towards the bent one.

SAXRD measurements of an aligned sample of **L3_G2** material at 30 deg. C revealed pattern similar to the one observed for **L2_G2** NPs, accordingly it was indexed assuming centered rectangular unit cell (2D). However, in contrast to the **L2_G2**

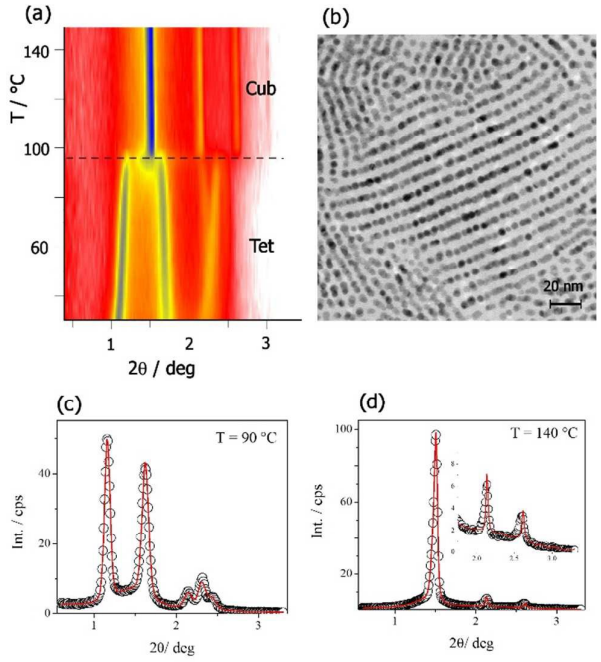

Figure 5. Structural characterization of **L3_G4** material. a) Temperature evolution of SAXRD patterns taken for annealed sample and b) corresponding TEM image. Comparison of modelled (red line) and measured (circles) SAXRD profile for (c) low and (d) high temperature structures.

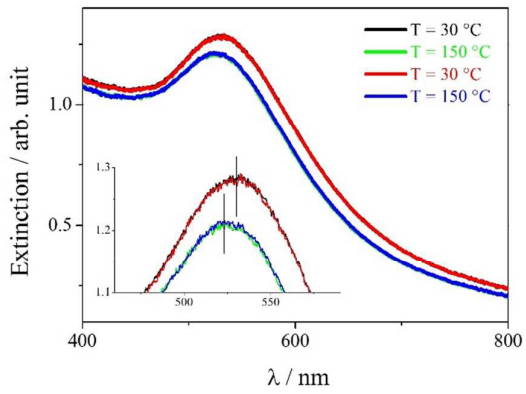

Figure 6. Temperature dependent absorption spectra in Vis range for **L3_G4** material.

sample, the unit cell parameters changed with temperature: from a=3.2 nm, c=15.3 nm at 30 °C to a=3.3 nm, c=14.1 nm at 120 °C.

TEM micrograph of an annealed **L3_G2** sample evidenced rows of NPs with 7.5 nm inter-row distance, corresponding to interlayer distance along *c* axis of the aggregate.

Above 120 °C the structure melted to an isotropic liquid – related pattern exhibited only one diffusive reflection indicating mean interparticle distance of 4.7 nm. It should be stressed that

XRD patterns recorded on cooling from isotropic liquid match very well to those collected on heating, thus we can conclude that isotropization is fully reversible. However, the transition is of long-to-short range order type, thus does not meet the requirement for precise control of nanoparticle spacing that is the aim of this study.

Also for **S5_L3** the transition from positionally ordered to liquid phase was observed. The SAXRD pattern of low temperature phase showed two relatively narrow signals, at 8.60 and 6.20 nm, which can be ascribed to long-range ordered lamellar structure. TEM imaging confirmed this phase assignment by revealing rows of NPs with inter-row spacing of ca. 8.5 nm, corresponding well to XRD measurements. Above 90 °C only one, diffusive signal at 7.52 nm was observed, indicating short-range positional order of the system.

For the last material, **L3_G4**, two distinct SAXRD patterns were observed below and above 95 °C (Fig. 5a), both can be ascribed to long-range ordered structures. For the low temperature phase the best fit for to the pattern (Fig. 5c) was obtained assuming 3D structure with tetragonal symmetry and unit cell parameters changing from a=5.47 and c=16.19 nm at 30 deg. C to a=5.76 and c=14.85 nm at 90 °C. The upper temperature phase was identified as body centered cubic (Fig. 5d) with lattice parameter a=8.25 nm at 100 deg. C and a=8.29 nm at 140 °C. Thus, **L3_G4** material exhibits structural reconfigurability between two long-range ordered phases as aimed in this study.

We have also investigated the influence of heating/cooling kinetics on nanoparticle rearrangement. Measurements of **L3_G4** material taken for different heating/cooling rates (up to 40 K/min) resulted in identical diffractograms. The same pattern of tetragonal phase was also found for the sample rapidly quenched from the cubic phase. This is a substantial progress in the view of previously reported reconfigurable aggregates of NPs, which required slow cooling in order to develop well defined structures.[15,48]

Finally, we have investigated the influence of the phase transition on the plasmonic resonance of **L3_G4** material. The UV-Vis extinction spectra were collected at 30 and 140 °C, corresponding to tetragonal and cubic structures, respectively. A clear, 8 nm shift of the plasmonic peak maximum was observed. Importantly, the shift was fully reversible.

Conclusions

We have demonstrated that it is possible to obtain dynamic nanoparticle material from densely packed plasmonic NPs covered with properly designed LC-ligands. The material can be relatively quickly switched between two long-range ordered states and due to dense packing of nanoparticles the observed structural reconfiguration translates to plasmonic switchability. Thus, we prove that the LC-NPs approach to active plasmonic systems should allow surpassing current limitations of nanoparticle-based tuneable metamaterials. Due to feasibility of the LC approach in future this strategy will be applied to other plasmonic NPs to increase their optical response.

Acknowledgements

WL and JM would like to acknowledge support from Polish National Science Centre, grant number UMO-2012/05/B/ST5/00725.

Notes and references

Electronic Supplementary Information (ESI) available: [details of any supplementary information available should be included here]. See DOI: 10.1039/b000000x/

1 Y. Sun, L. Jiang, L. Zhong, Y. Jiang, and X. Chen, *Nano Res.*, 2015, **8**, 406–417.
2 O. Hess, J. B. Pendry, S. A. Maier, R. F. Oulton, J. M. Hamm, and K. L. Tsakmakidis, *Nat. Mater.*, 2012, **11**, 573–584.
3 A. T. Fafarman, S.-H. Hong, H. Caglayan, X. Ye, B. T. Diroll, T. Paik, N. Engheta, C. B. Murray, and C. R. Kagan, *Nano Lett.*, 2013, **13**, 350–7.
4 M. Nguyen, X. Sun, E. Lacaze, P. M. Winkler, A. Hohenau, J. R. Krenn, C. Bourdillon, A. Lamouri, J. Grand, G. Lévi, L. Boubekeur-Lecaque, C. Mangeney, and N. Félidj, *ACS Photonics*, 2015, **2**, 1199–1208.
5 M. Ardini, F. Giansanti, L. Di Leandro, G. Pitari, A. Cimini, L. Ottaviano, M. Donarelli, S. Santucci, F. Angelucci, and R. Ippoliti, *Nanoscale*, 2014, **6**, 8052–61.
6 M. Wang, L. He, W. Xu, X. Wang, and Y. Yin, *Angew. Chemie Int. Ed.*, 2015, **54**, 7077–7081.
7 L. De Sio, A. Cunningham, V. Verrina, C. M. Tone, R. Caputo, T. Bürgi, and C. Umeton, *Nanoscale*, 2012, **4**, 7619–23.
8 M. Gajc, H. B. Surma, A. Klos, K. Sadecka, K. Orlinski, A. E. Nikolaenko, K. Zdunek, and D. A. Pawlak, *Adv. Funct. Mater.*, 2013, **23**, 3443–3451.
9 L. Wang and Q. Li, *Adv. Funct. Mater.*, 2015, 10.1002/adfm.201502071.
10 L. Xu, W. Ma, L. Wang, C. Xu, H. Kuang, and N. A. Kotov, *Chem. Soc. Rev.*, 2013, **42**, 3114.
11 L. De Sio, T. Placido, R. Comparelli, M. Lucia Curri, M. Striccoli, N. Tabiryan, and T. J. Bunning, *Prog. Quantum Electron.*, 2015, **41**, 23–70.
12 W. B. Rogers and V. N. Manoharan, *Science (80-.).*, 2015, **347**, 639–642.
13 M. M. P. Arnob, F. Zhao, J. Zeng, G. M. Santos, M. Li, and W.-C. Shih, *Nanoscale*, 2014.
14 N. Jiang, Q. Ruan, F. Qin, J. Wang, and H.-Q. Lin, *Nanoscale*, 2015, **7**, 12516–26.
15 K. Heo, C. Miesch, T. Emrick, and R. C. Hayward, *Nano Lett.*, 2013, **13**, 5297–302.
16 Y. Zhao, K. Thorkelsson, A. J. Mastroianni, T. Schilling, J. M. Luther, B. J. Rancatore, K. Matsunaga, H. Jinnai, Y. Wu, D. Poulsen, J. M. J. Fréchet, A. P. Alivisatos, and T. Xu, *Nat. Mater.*, 2009, **8**, 979–85.
17 Y. Kim, J. Zhu, B. Yeom, M. Di Prima, X. Su, J.-G. Kim, S. J. Yoo, C. Uher, and N. a Kotov, *Nature*, 2013, **500**, 59–63.
18 V. Sashuk, K. Winkler, A. Żywociński, T. Wojciechowski, E. Górecka, and M. Fiałkowski, *ACS Nano*, 2013, **7**, 8833–9.
19 I. Lagzi, B. Kowalczyk, D. Wang, and B. a Grzybowski, *Angew. Chem. Int. Ed. Engl.*, 2010, **49**, 8616–9.
20 R. Klajn, K. J. M. Bishop, and B. A. Grzybowski, *Proc. Natl. Acad. Sci. U. S. A.*, 2007, **104**, 10305–9.
21 S.-H. Jeong, J. W. Lee, D. Ge, K. Sun, T. Nakashima, S. Il Yoo, A. Agarwal, Y. Li, and N. a. Kotov, *J. Mater. Chem.*, 2011, **21**, 11639.
22 A. Tao, P. Sinsermsuksakul, and P. Yang, *Nat. Nanotechnol.*, 2007, **2**, 435–40.
23 Q. Liu, Y. Cui, D. Gardner, X. Li, S. He, and I. I. Smalyukh, *Nano Lett.*, 2010, **10**, 1347–53.
24 K. Slyusarenko, D. Constantin, B. Abécassis, P. Davidson, and C. Chanéac, *J. Mater. Chem. C*, 2014, **2**, 5087.
25 Q. Liu, Y. Yuan, and I. I. Smalyukh, *Nano Lett.*, 2014, **14**, 4071–7.
26 L. Wang, K. G. Gutierrez-Cuevas, H. K. Bisoyi, J. Xiang, G. Singh, R. S. Zola, S. Kumar, O. D. Lavrentovich, A. Urbas, and Q. Li, *Chem. Commun.*, 2015, **51**, 15039–42.
27 K. G. Gutierrez-Cuevas, L. Wang, C. Xue, G. Singh, S. Kumar, A. Urbas, and Q. Li, *Chem. Commun.*, 2015, **51**, 9845–8.
28 J. M. D. Lane and G. S. Grest, *Nanoscale*, 2014, **6**, 5132–7.
29 D. Ortiz, K. L. Kohlstedt, T. D. Nguyen, and S. C. Glotzer, *Soft Matter*, 2014, **10**, 3541–52.
30 R. Guo, Z. Liu, X.-M. Xie, and L.-T. Yan, *J. Phys. Chem. Lett.*, 2013, **4**, 1221–1226.
31 T. D. Nguyen, E. Jankowski, and S. C. Glotzer, *ACS Nano*, 2011, **5**, 8892–903.
32 M. M. Wójcik, M. Olesińska, M. Sawczyk, J. Mieczkowski, and E. Górecka, *Chemistry*, 2015, **21**, 10082–8.
33 D. Jishkariani, B. T. Diroll, M. Cargnello, D. R. Klein, L. A. Hough, C. B. Murray, and B. Donnio, *J. Am. Chem. Soc.*, 2015, **137**, 10728–10734.
34 L. Cseh, X. Mang, X. Zeng, F. Liu, G. H. Mehl, G. Ungar, and G. Siligardi, *J. Am. Chem. Soc.*, 2015, **137**, 12736–12739.
35 J. M. Wolska, D. Pociecha, J. Mieczkowski, and E. Górecka, *Chem. Commun.*, 2014, **50**, 7975–8.
36 W. Lewandowski, M. Wójcik, and E. Górecka, *Chemphyschem*, 2014, **15**, 1283–95.
37 C. Blanc, D. Coursault, and E. Lacaze, *Liq. Cryst. Rev.*, 2013, **1**, 83–109.
38 O. Stamatoiu, J. Mirzaei, X. Feng, and T. Hegmann, *Top. Curr. Chem.*, 2012, **318**, 331–93.
39 G. L. Nealon, R. Greget, C. Dominguez, Z. T. Nagy, D. Guillon, J.-L. Gallani, and B. Donnio, *Beilstein J. Org. Chem.*, 2012, **8**, 349–70.
40 S. Saliba, C. Mingotaud, M. L. Kahn, and J.-D. Marty, *Nanoscale*, 2013, **5**, 6641–61.
41 H. K. Bisoyi and S. Kumar, *Chem. Soc. Rev.*, 2011, **40**, 306–19.
42 J. Dintinger, B.-J. Tang, X. Zeng, F. Liu, T. Kienzler, G. H. Mehl, G. Ungar, C. Rockstuhl, and T. Scharf, *Adv. Mater.*, 2013, **25**, 1999–2004.
43 W. Lewandowski, D. Constantin, K. Walicka, D. Pociecha, J. Mieczkowski, and E. Górecka, *Chem. Commun.*, 2013, **49**, 7845–7.
44 S. Umadevi, X. Feng, and T. Hegmann, *Adv. Funct. Mater.*, 2013, **23**, 1393–1403.
45 C. Xue, J. Xiang, H. Nemati, H. K. Bisoyi, K. Gutierrez-Cuevas, L. Wang, M. Gao, S. Zhou, D. Yang, O. D. Lavrentovich, A. Urbas, and Q. Li, *Chemphyschem*, 2015, **16**, 1852–6.
46 A. Zep, M. M. Wojcik, W. Lewandowski, K. Sitkowska, A. Prominski, J. Mieczkowski, D. Pociecha, and E. Gorecka, *Angew. Chem. Int. Ed. Engl.*, 2014, **53**, 13725–8.
47 M. M. Wojcik, M. Gora, J. Mieczkowski, J. Romiszewski, E. Gorecka, and D. Pociecha, *Soft Matter*, 2011, **7**, 10561.
48 W. Lewandowski, M. Fruhnert, J. Mieczkowski, C. Rockstuhl, and E. Górecka, *Nat. Commun.*, 2015, **6**, 6590.
49 M. M. Wojcik, M. Gora, J. Mieczkowski, J. Romiszewski, E. Gorecka, and D. Pociecha, *Soft Matter*, 2011, **7**, 10561.
50 G. Si, Y. Zhao, E. Leong, and Y. Liu, *Materials*, 2014, **7**, 1296–1317.
51 K. Fan and W. J. Padilla, *Mater. Today*, 2015, **18**, 39–50.
52 Y. Chen and X. Wang, *Mater. Lett.*, 2008, **62**, 2215–2218.
53 M. Brust, M. Walker, D. Bethell, D. J. Schiffrin, and R. Whyman, *J. Chem. Soc. Chem. Commun.*, 1994, 801.
54 E. Dzik, J. Mieczkowski, E. Gorecka, and D. Pociecha, *J. Mater. Chem.*, 2005, 1255–1262.
55 M.-C. Daniel and D. Astruc, *Chem. Rev.*, 2004, **104**, 293–346.
56 C. Xue, Y. Xue, L. Dai, A. Urbas, and Q. Li, *Adv. Opt. Mater.*, 2013, **1**, 581–587.

57 L. Cseh and G. H. Mehl, *J. Am. Chem. Soc.*, 2006, **128**, 13376–7.